Generation of bulk nanobubbles using a high-shear rotor-stator device

Jadhav, Anand; Ferraro, Gianluca; Barigou, Mostafa

DOI:
10.1021/acs.iecr.1c01233

Generation of bulk nanobubbles using a high-shear rotor-stator device

Ananda J. Jadhav, Gianluca Ferraro, Mostafa Barigou*

School of Chemical Engineering, University of Birmingham, Edgbaston, Birmingham B15 2TT, United Kingdom

Abstract

We describe the generation of bulk nanobubbles in pure water using a high-shear rotor-stator device. The technique can be used in batch mode to produce relatively small volumes of bulk nanobubble suspension on the order of hundreds of milliliters or in semi-continuous mode to process much larger volumes on the order of tens of liters, making it more amenable for scale-up. The design of the stator influences the effectiveness of nanobubble generation. The two operating modes generate comparable concentrations of bulk nanobubbles when using similar rotor-stator configurations and hydrodynamic regime. The bulk nanobubble yield can be enhanced up to a limit through greater energy input, longer operating times, higher water operating temperatures to release more dissolved air or by continuous additional sparging of air or nitrogen. Sparging CO_2, however, annihilates the generation of bulk nanobbubbles as it forms carbonic acid which is detrimental to the stability of bulk nanobubbles.

*Corresponding author; Email: m.barigou@bham.ac.uk

1. Introduction

Bulk nanobubbles (BNBs) have been reported in many recent experimental studies, and they have also been the subject of a number of computational modelling investigations. Diverse methods have been used to produce BNBs including acoustic cavitation,[1–3] hydrodynamic cavitation,[4–17] water solvent mixing,[18–20] microfluidics,[21] periodic pressure change method,[22] nano-membranes,[23–26] and pressure induced supersaturation.[27]

Acoustic cavitation: Acoustic cavitation has been employed to generate BNBs in pure water and in aqueous organic solvent solutions. Acoustic cavitation involves the generation, expansion, growth, and adiabatic collapse of microscopic cavities or microbubbles. We recently showed that batch acoustic cavitation implemented using an ultrasound probe sonicator, can be effective in producing stable BNBs in pure water as well as in ethanol-water mixtures.[2,3] Cavitation leads to the generation of BNBs via two possible routes: (i) simultaneous generation of microbubbles and nanobubbles; and (ii) subsequently microbubbles may gradually shrink in size with increasing surface charge density to become nanobubbles. It is not clear a priori whether both of these events occur concurrently and, if so, which one is predominant. On increasing sonication time (i.e., ultrasound energy input), the population of BNBs produced increased substantially. It was also shown that dissolved gas was needed for the generation of BNBs. Yasuda et al.[1] also used ultrasonic cavitation to generate BNBs in pure water. More recently, we successfully extended the application of acoustic cavitation to the generation of BNBs in semi-continuous mode, which is more amenable to large scale processing.[28]

Hydrodynamic cavitation: Hydrodynamic cavitation is concerned with the nucleation of bubbles in a flowing fluid due to a reduction in local pressure below the liquid vapour pressure. Typical examples include flow through a nozzle, orifice, venture or rotary pump. Ushikubo et al.[6] used a micro/nanobubble generator in which liquid and gas were mixed using a magnetic gear pump and allowed to pass through a nozzle to generate microbubbles and nanobubbles. Similarly, Matsuki at al.[7], Liu et al.[8], Matsuno et al.[9] and Nakatake et al.[10] used a nozzle for generating BNBs. Furthermore, turbulent flow can also lead to the generation of microbubbles and nanobubbles due to turbulent pressure fluctuations. Ushida, et al.[11,12] and Ebina et al.[13] utilized a Taylor-Couette type BNB generator. Similarly, Ohgaki et al.[4] proposed a zero clearance rotary pump to generate BNBs, while Calgaroto et al.[14] used a needle valve. A

number of commercial BNB generators based on this principle exist on the market including IDEC ultrafine bubble generator,[15] OxydoserTM bubble generator,[16] OK fine bubble generator.[17] In conclusion, whilst hydrodynamic cavitation shows promise for BNB generation, there are no systematic studies of the method available.

Water-organic solvent mixing: Mixing of water miscible organic solvents such as simple alcohols (methanol, ethanol, propanol), small ketone (acetone) or organosulfur compound (dimethyl sulfoxide) and water equilibrated with atmospheric gases causes supersaturation of dissolved gases which are less soluble in the mixture than in the individual components and, thus, leads to nucleation and spontaneous formation of stable BNBs. We recently studied the spontaneous formation of BNBs in aqueous solutions of different organic solvents (methanol, ethanol, propanol, acetone, dimethyl sulfoxide and formamide).[29] The extensive results obtained showed that the bubble number density increases sharply with solvent content, reaching a maximum at an intermediate solvent concentration depending on the type of solvent. The maximum was shown to coincide with maximum gas oversaturation of water. Similar observations have been reported by Millare and Basilia.[19,20] Beyond the point of maximum BNB generation, the bubble number density falls off sharply with no BNBs forming beyond a certain solvent concentration which depends on the type of solvent used. A pure organic solvent acts as a gas sink removing any excess gas from the solution and thus does not form BNBs. In an aqueous solvent solution, the gas solubility of the solvent relative to water is a determining factor in the number of BNBs formed. Experiments in which degassed water and degassed ethanol were mixed under vacuum produced no BNBs, confirming thus that BNB generation depends on the availability of dissolved gas in water and ethanol.[28]

Microfluidics: In a microfluidic device, there are a number of factors at play including high shear, intense turbulence, collision effects and hydrodynamic cavitation which may be responsible for the formation of microbubbles which shrink to form BNBs, or may even lead directly to the formation of BNBs. Peyman et al.[30] used a flow focusing microfluidic device of 25 μm width and 50 μm depth operating at 15 psi pressure, to produce BNBs of about 250 nm diameter with a bubble number density of 10^{11}-10^{12} bubbles.mL^{-1}. In a recent study, we employed a microfluidic device consisting of a 75 μm microchannel to generate BNBs in pure water, using high operating pressures in the range 300-1500 bar and volumetric flowrates in the range 150-300 mL.min^{-1}.[21] The operating mean velocity in the microchannel was in the

range 440-880 m s^{-1}. Whilst the shape of the bubble size distribution was more or less unaffected and the mean bubble diameter remained constant at ~130 nm, the bubble number density increased considerably with operating pressure.

Periodic pressure change method: Recently, Wang et al.[22] introduced a periodic pressure change method to produce the N_2, O_2 or CO_2 BNBs in pure water. The principle of generation of BNBs is based on the periodic change of internal pressure in a U-tube containing water and gas. The periodic change in pressure causes a change in gas solubility, which leads to the production of BNBs.

*Nano-membrane*s: Porous membranes have been utilized to generate BNBs of air, nitrogen or oxygen in pure water.[23–25] In this method, pressurized gas is injected through a tubular ceramic membrane with ideally uniform nanopores to induce BNBs in water. Successful applications have reported by Kukizaki and Goto,[23] Oh et al.[26] and Ahmed et al.[25]

Kukizaki and Goto[23] used a Shirasu-porous-glass membrane of 43-85 nm pores to generate BNBs in water in the range 360-720 nm, almost an order of magnitude larger than the average pore diameter. Smaller BNBs, however, should be possible with finer membranes and/or optimised processing conditions. More recently, Oh et al.[26] used a membrane to produce hydrogen BNBs in gasoline with a concentration, mean size and zeta potential of 1.125×10^9 bubbles.mL^{-1}, 159 nm and −30 mV, respectively. The results, however, may be suspect given the likelihood of impurities present in gasoline. Similarly, Ahmed et al.[25] showed that the injection pressure in a ceramic nozzle reduces the size of BNBs produced.

Pressure induced supersaturation: We recently introduced a new technique for generating bulk nanobubble suspensions based on Henry's law which states that the amount of dissolved gas in a liquid is proportional to its partial pressure above the liquid.[27] This principle which forms the basis of vacuum degasification has been exploited to produce stable BNBs in pure water of 120 nm diameter at concentrations of 10^9 bubble.mL^{-1}, through successive expansion/compression strokes inside a sealed syringe. An automated variant was proposed which has potential for scale-up production of BNB suspensions. The technique is relatively 'clean' and may find applications in areas such as healthcare.

In conclusion, though BNBs have been successfully generated by all the methods described above, results remain scarce and more detailed investigations are needed to study the properties of BNBs obtained and optimise their production by these techniques. To meet the needs of the various industrial applications involving BNBs, novel efficient methods are still required which are 'clean', can produce concentrated BNB suspensions, are cost effective and amenable to scale-up and process control.

In this paper, we study and compare the generation of BNBs in pure water using batch and semi-continuous high-shear rotor-stator devices with and without additional sparging of gas. We, thus, study the effects of different gases (air, N_2, and CO_2). We also investigate the effects of operating parameters such as rotor speed, energy input, operating temperature, processing time and stator design on the BNB suspensions formed.

2. Experimental

2.1 Materials

Ultrapure water (type-1), henceforth referred to as simply pure water, from a Millipore purification system (Avidity Science, UK), of electrical conductivity 0.055 $\mu S.cm^{-1}$ and pH 6.7 at a temperature of 20 ˚C, was used in all experiments. Dry air, nitrogen and carbon dioxide gases of purity >99.5%, were supplied by BOC (UK). All glassware was cleaned by immersion for 30 min in a 10% aqueous solution of potassium hydroxide (KOH, Sigma Aldrich, UK) placed inside an ultrasonic bath, followed by rinsing with ultrapure water, drying in a microwave oven and flushing with a stream of high-purity dry nitrogen gas. Prior to experimentation, the purified water and all stock solutions were examined using the Nanosight instrument (described further below) employed for the measurement of BNBs, to ascertain that no significant levels of nanoscale impurities were present. In all cases, the BNB suspensions formed were stored in 20 mL air-tight glass vials for further analysis.

2.2 Methods

We used both a batch and a semi-continuous high-shear rotor-stator device to generate BNB suspensions in pure water. To check the effects of type of gas on the generation of BNBs in pure water, a different gas (air, N_2 or CO_2) was continuously sparged close to the rotor-stator head at a fixed optimum flowrate of 1 L min^{-1}; lower gas flowrates were not effective whilst

higher flowrates flooded the rotor-stator and caused the pumping action of the rotor-stator to fail.

2.2.1 Batch high-shear rotor-stator device system (BAS)

Here, bulk nanobubbles were generated using a batch high-shear rotor-stator device (Silverson Laboratory Mixers L5M-A model, Silverson Machines Ltd, UK), as schematically represented in Figure 1 (a). The mixer device was equipped with a single 4-blade rotor of diameter 15.60 mm, located inside a stator of 15.80 mm inner diameter and 19 mm outer diameter. Five different stator designs were used, as shown in Figure 1 (b), details of which are summarised in Table 1. The rotor was driven by a 1 hp (0.75 kW) variable speed motor with a maximum speed of 10000 rpm. The experimental set-up was used to generate 200 mL of BNB suspension in pure water with and without added air sparging.

2.2.2 Semi-continuous high-shear rotor-stator device system (SCS)

Generation of bulk nanobubbles was also investigated in a semi-continuous high-shear rotor-stator device (Silverson Machines Ltd, UK), as schematically represented in Figure 2 (a). The device was equipped with a single 4-blade rotor of 38 mm diameter, located inside a stator of 38.5 mm inner diameter and 41.25 mm outer diameter. Five different stator designs were used, as shown in Figure 2 (b), details of which are given in Table 1. The rotor was driven by a 1 hp (0.75 kW) variable speed motor with a maximum speed of 10000 rpm. The experimental set-up was used to generate 10 L of BNB suspension by recirculating pure water inside a 20 L stainless steel vessel (Figure 2(a)). BNB production was conducted with and without added sparging of air.

2.3 Characterization of BNB suspensions

The size distribution and the number density of BNBs were measured using a nanoparticle tracking analysis (NTA) instrument (NanoSight NS300, Malvern-UK). NTA tracks the Brownian motion of nanoparticles and is ideally suited for real-time analysis of polydisperse systems ranging from 10 to 2000 nm in size and 10^7 to 10^9 particles.mL^{-1} in concentration. It is superior to dynamic light scattering (DLS) whose measurements are based on the intensity of scattered light and is, thus, biased towards large particles.[2] Standard suspensions of solid latex nanospheres were used to verify the accuracy and precision of the NTA system and to adjust the instrument settings accordingly, prior to the analysis of nanobubble samples. The

zeta potential of the nanobubbles was measured using a Zetasizer Nano ZSP instrument (ZEN5600, Malvern-UK). These measurement techniques and their protocols are discussed in more detail in our recent papers.[2,3]

2.4 Analysis of impurities and contamination

To verify that the BNBs observed were not the result of foreign matter, the BNB suspensions were analysed by inductive coupled plasma mass spectroscopy (ICPMS) and gas chromatography mass spectroscopy (GCMS) to determine the level of any metal or organic contamination introduced by the process. ICPMS analysis revealed that the level of metal impurities was negligible and similar to that contained in pure water. Similarly, analysis by GCMS showed that the mass spectrum of the BNB suspensions was identical to that of pure water.

3. Results and discussion

3.1 Generation of BNBs in pure water

The working mechanism of a high-shear rotor-stator device is based on the generation of high shear, intense turbulence, collision effects and perhaps most importantly hydrodynamic cavitation which is probably the primary mechanism responsible for the formation of microbubbles. During agitation, a white cloud of microbubbles forms which on cessation of agitation could be seen to slowly rise to the surface and disappear. In the process, some of these microbubbles may shrink to form BNBs. At the same time, the onset of cavitation may also lead directly to the formation of BNBs.

3.2 Effects of rotor-stator design

BNB suspensions were produced in the BAS and SCS systems using different types of stator, to study the effects of stator design on the generation of BNBs. The characteristics, in terms of bubble size distribution, mean bubble diameter, bubble number density and zeta potential, of the BNB suspensions generated using BAS and SCS in pure water are depicted in Figure 3 and Figure 4, respectively. In each case, the rotor-stator device was run continuously at room temperature for 30 min at a rotor speed of 10000 rpm.

The bubble size distributions obtained using different stators are similar and the mean bubble diameter and zeta potential are approximately the same, but the bubble number density is markedly different, as shown in Figure 3 and Figure 4. For BAS, the bubble number density seems to correlate with the total opening area of the stator (see Table 1), i.e. the larger the total area of the openings, the larger the nanobubble concentration generated. However, this is not the case for SCS, which suggests that this is a simplistic interpretation of the complex phenomena occurring in the high-shear region of the device which lead to the formation of BNBs. Some earlier studies mainly targeted at the process of emulsification, investigated in some detail via experimental measurements and computational fluid mechanics simulations the complex flow field generated by different rotor-stator configurations.[31–35] It ensues that there are other important parameters which influence the flow field in the vicinity of the rotor-stator such as the shape and size of the openings and their spacing as well as stator thickness, in addition to operational parameters including rotor speed, energy input, liquid physical properties and the onset of hydrodynamic cavitation.

For example, the power number is proportional to the flowrate through the stator openings while the flowrate correlates directly with the total opening area. Stators with a small opening spacing are expected to dissipate more energy in the rotor swept volume and opening region than those with large opening spacing. However, a large opening spacing dissipates more energy in the bulk region suggesting it is more suitable for bulk agitation. Narrower openings allow better transfer of the tangential momentum from the rotor to the surrounding fluid, hence there is less pumping action as the fluid moves in the tangential as opposed to the radial direction.[34,35] The total energy dissipation was determined as a function of operating time at 10000 rpm for each stator in both batch and semi-continuous flow, as depicted in Figure 5, by measuring in each case the rise in liquid temperature. The difference between the different stator designs is small but significant. However, for both devices, it does not correlate with stator performance in terms of bubble number density generated, as shown in Figures 3 and 4. Given the complex nature of the highly turbulent flow field in which the BNBs are formed (12000< Reynolds number <240000), it is a priori difficult to speculate on which of these factors are more influential in terms of BNB generation. In the rest of this study we used stators BS5 and CS5 which produced most BNBs in each case.

3.3 Effects of operating rotor speed

The characteristics, in terms of bubble size distribution, mean bubble diameter, bubble number density and zeta potential, of the BNB suspensions generated by BAS and SCS in pure water are presented as a function of rotor speed in Figure 6 and Figure 7, respectively. In both batch and semi-continuous operation at room temperature for 30 min, rotor speed seems to have little effect on the bubble size distribution and mean bubble diameter. The bubble number density, however, increases considerably with rotor speed. The zeta potential of the nanobubbles remains unchanged within experimental error at about −25 mV. This is expected since the zeta potential of a suspension of nano-entities (nanoparticles or nanobubbles) is independent of the number of nano-entities in the suspension.[36]

A higher rotor speed increases the fluid velocity in the rotor-stator gap which intensifies turbulence and reduces the cavitation number and, hence, enhances cavitation resulting in more nanobubbles. In general, the higher the rotor speed, the more tangential the flow exiting the rotor-stator through the openings becomes and vice versa.[34] In an emulsification process, a more tangential flow is associated with the formation of smaller droplet sizes due to the dominating breakup mechanism caused by fluid impingement on the stator.[33,34] It is not a priori obvious, however, whether or how this particular phenomenon may affect BNB generation since the mean bubble diameter seems to be independent of rotor speed, while the bubble number density increases substantially.

3.4 Effects of operating time

The effects of operating time on the generation of BNBs in pure water were checked by conducting experiments for different operating times, all at room temperature and maximum rotor speed of 10000 rpm. Results are shown in Figure 8. The mean diameter remains more or less unaffected whereas the bubble number density rises with increasing run time, as increasingly more energy is dissipated (Figure 9). However, the curve does not reach a plateau even after 60 min and continues to increase, which implies that more released air is still available in the water which requires more operating time (i.e. more energy input) to convert into BNBs. These results seem to suggest that the BNBs either form using dissolved air as a result of cavitation or using air ingested from the surroundings as a result of turbulence.

3.5 Effects of operating temperature

Experiments were conducted to study the effects of water temperature on the generation of BNBs. Using the BAS device at an operating at a speed of 10000 rpm, experiments were performed with temperature controlled to within ±3 °C at values of 10, 20, 30, 40 and 50 °C, using an external recirculating cooler. BNB samples were withdrawn at 10 min time intervals and analysed. Results depicted in Figure 10 (a)-(b), show that whilst the mean bubble diameter is not significantly affected by temperature or operating time, a higher temperature and longer operating time lead to considerably larger bubble number density.

In case of the SCS, temperature control during operation was difficult and could not be implemented. Nonetheless, similar experiments were conducted for different starting water temperatures, namely 5, 20 and 50 °C. Results presented in Figure 10 (c)-(d) show similar effects as for the batch device. These results show that more BNBs are generated at higher temperatures because air solubility is lower and the amount of air available is higher.

3.6 Effects additional air sparging

In both batch and semi-continuous systems, additional air sparging leads to more BNB generation, as shown in Figure 11. Additional air sparging causes water to remain saturated which increases the available air for BNB generation, hence, enabling the formation of more BNBs, well above the bubble concentration obtained in pure water without additional air sparging. This result corroborates the above finding that the generation of BNBs is governed by the amount of available air.

3.7 Effects of type of gas

The effects of type of dissolved gas on the formation of BNBs, were explored by separately sparging air, nitrogen or carbon dioxide in pure water during the operation of the BAS and SCS devices. Prior to the experiment, the gas is continuously sparged into the water for 15 min, and thereafter during BNB generation. Results plotted in Figure 12 show that the BNB size is not affected by the type of gas. However, the effects on bubble number density are remarkable. In both devices, more BNBs are generated with air than with N_2 than with CO_2. The difference in bubble number density for the inert gases which do not react with water, can be attributed to the difference in water solubility of these gases, *i.e.* air > N_2. In the case of CO_2, however, the

bubble number density is very low because CO_2 is highly reactive with water and forms carbonic acid (H_2CO_3) which reduces the pH of the solution (~ pH 4). We have previously shown that BNBs are unstable in acidic media, which seems to explain why BNBs do not in CO_2 sparged water.[21]

In conclusion, the two devices batch and semi-continuous seemed to perform equally well under the various conditions of the tests conducted above. The semi-continuous systems, however, has the advantage of being amenable to scale-up and high-volume production of BNB suspensions.

Conclusions

A high-shear rotor stator device for producing bulk nanobubble suspensions in pure water has been described. The technique can be used in either batch mode to generate small volumes on the order of hundreds of milliliters or in semi-continuous mode to process large volumes on the order of tens of litres, making it more amenable for scale-up. Both modes of operation can generate up to ~ 2×10^8 bubble.mL^{-1} in pure water. The design of the stator influences the nanobubble generation effectiveness of the method. The two operating modes generate comparable concentrations of bulk nanobubbles when using similar rotor-stator configurations and hydrodynamic regime. The bulk nanobubble yield in pure water can be enhanced up to a maximum of ~ 2×10^8 bubble.mL^{-1} through greater energy input, longer operating times or higher water operating temperatures to release more dissolved air. The type of dissolved gas has significant on BNB generation. The bubble number density can be enhanced by continuous additional sparging of air. Sparging nitrogen increases the bubble number density less than air, the difference being attributed to the difference in the water solubility of these gases. Sparging CO_2, however, completely suppresses the formation of bulk nanobbubbles as it forms carbonic acid which is detrimental to their stability.

Acknowledgements

This work was supported by EPSRC Grant EP/L025108/1.

References

(1) Yasuda, K.; Matsushima, H.; Asakura, Y. Generation and Reduction of Bulk Nanobubbles by Ultrasonic Irradiation. *Chem. Eng. Sci.* **2019**, *195*, 455–461. https://doi.org/10.1016/j.ces.2018.09.044.

(2) Nirmalkar, N.; Pacek, A. W.; Barigou, M. On the Existence and Stability of Bulk Nanobubbles. *Langmuir* **2018**, *34* (37), 10964–10973. https://doi.org/10.1021/acs.langmuir.8b01163.

(3) Nirmalkar, N.; Pacek, A. W.; Barigou, M. Bulk Nanobubbles from Acoustically Cavitated Aqueous Organic Solvent Mixtures. *Langmuir* **2019**, *35* (6), 2188–2195. https://doi.org/10.1021/acs.langmuir.8b03113.

(4) Ohgaki, K.; Khanh, N. Q.; Joden, Y.; Tsuji, A.; Nakagawa, T. Physicochemical Approach to Nanobubble Solutions. *Chem. Eng. Sci.* **2010**, *65* (3), 1296–1300. https://doi.org/10.1016/j.ces.2009.10.003.

(5) Oh, S. H.; Kim, J.-M. Generation and Stability of Bulk Nanobubbles. *Langmuir* **2017**, *33* (15), 3818–3823. https://doi.org/10.1021/acs.langmuir.7b00510.

(6) Ushikubo, F. Y.; Furukawa, T.; Nakagawa, R.; Enari, M.; Makino, Y.; Kawagoe, Y.; Shiina, T.; Oshita, S. Evidence of the Existence and the Stability of Nano-Bubbles in Water. *Colloids Surf. Physicochem. Eng. Asp.* **2010**, *361* (1), 31–37. https://doi.org/10.1016/j.colsurfa.2010.03.005.

(7) Matsuki, N.; Ishikawa, T.; Ichiba, S.; Shiba, N.; Ujike, Y.; Yamaguchi, T. Oxygen Supersaturated Fluid Using Fine Micro/Nanobubbles. *Int. J. Nanomedicine* **2014**, *9*, 4495–4505. https://doi.org/10.2147/IJN.S68840.

(8) Liu, S.; Kawagoe, Y.; Makino, Y.; Oshita, S. Effects of Nanobubbles on the Physicochemical Properties of Water: The Basis for Peculiar Properties of Water Containing Nanobubbles. *Chem. Eng. Sci.* **2013**, *93*, 250–256. https://doi.org/10.1016/j.ces.2013.02.004.

(9) Matsuno, H.; Ohta, T.; Shundo, A.; Fukunaga, Y.; Tanaka, K. Simple Surface Treatment of Cell-Culture Scaffolds with Ultrafine Bubble Water. *Langmuir* **2014**, *30* (50), 15238–15243. https://doi.org/10.1021/la5035883.

(10) Nakatake, Y.; Kisu, S.; Shigyo, K.; Eguchi, T.; Watanabe, T. Effect of Nano Air-Bubbles Mixed into Gas Oil on Common-Rail Diesel Engine. *Energy* **2013**, *59*, 233–239. https://doi.org/10.1016/j.energy.2013.06.065.

(11) Ushida, A.; Hasegawa, T.; Nakajima, T.; Uchiyama, H.; Narumi, T. Drag Reduction Effect of Nanobubble Mixture Flows through Micro-Orifices and Capillaries. *Exp. Therm. Fluid Sci.* **2012**, *39*, 54–59. https://doi.org/10.1016/j.expthermflusci.2012.01.008.

(12) Ushida, A.; Hasegawa, T.; Takahashi, N.; Nakajima, T.; Murao, S.; Narumi, T.; Uchiyama, H. Effect of Mixed Nanobubble and Microbubble Liquids on the Washing Rate of Cloth in an Alternating Flow. *J. Surfactants Deterg.* **2012**, *15* (6), 695–702. https://doi.org/10.1007/s11743-012-1348-x.

(13) Ebina, K.; Shi, K.; Hirao, M.; Hashimoto, J.; Kawato, Y.; Kaneshiro, S.; Morimoto, T.; Koizumi, K.; Yoshikawa, H. Oxygen and Air Nanobubble Water Solution Promote the Growth of Plants, Fishes, and Mice. *PloS One* **2013**, *8* (6), e65339. https://doi.org/10.1371/journal.pone.0065339.

(14) Calgaroto, S.; Wilberg, K. Q.; Rubio, J. On the Nanobubbles Interfacial Properties and Future Applications in Flotation. *Miner. Eng.* **2014**, *60*, 33–40. https://doi.org/10.1016/j.mineng.2014.02.002.

(15) IDEC Global : Ultrafine Bubble Generation Technology http://www.idec.com/home/finebubble/index.html (accessed Mar 25, 2021).

(16) OxyDoser^{TM} PUREair http://www.oxydoser.com/oxydoser-pureair.html (accessed Mar 25, 2021).

(17) Fine Bubble OK Brand Generators https://www.finebubble-ok.com/ (accessed Mar 25, 2021).

(18) Qiu, J.; Zou, Z.; Wang, S.; Wang, X.; Wang, L.; Dong, Y.; Zhao, H.; Zhang, L.; Hu, J. Formation and Stability of Bulk Nanobubbles Generated by Ethanol-Water Exchange. *Chemphyschem Eur. J. Chem. Phys. Phys. Chem.* **2017**, *18* (10), 1345–1350. https://doi.org/10.1002/cphc.201700010.

(19) Millare, J. C.; Basilia, B. A. Nanobubbles from Ethanol-Water Mixtures: Generation and Solute Effects via Solvent Replacement Method. *ChemistrySelect* **2018**, *3* (32), 9268–9275. https://doi.org/10.1002/slct.201801504.

(20) Millare, J. C.; Basilia, B. A. Dispersion and Electrokinetics of Scattered Objects in Ethanol-Water Mixtures. *Fluid Phase Equilibria* **2019**, *481*, 44–54. https://doi.org/10.1016/j.fluid.2018.10.013.

(21) Nirmalkar, N.; Pacek, A. W.; Barigou, M. Interpreting the Interfacial and Colloidal Stability of Bulk Nanobubbles. *Soft Matter* **2018**, *14* (47), 9643–9656. https://doi.org/10.1039/C8SM01949E.

(22) Wang, Q.; Zhao, H.; Qi, N.; Qin, Y.; Zhang, X.; Li, Y. Generation and Stability of Size-Adjustable Bulk Nanobubbles Based on Periodic Pressure Change. *Sci. Rep.* **2019**, *9* (1), 1118. https://doi.org/10.1038/s41598-018-38066-5.

(23) Kukizaki, M.; Goto, M. Size Control of Nanobubbles Generated from Shirasu-Porous-Glass (SPG) Membranes. *J. Membr. Sci.* **2006**, *281* (1), 386–396. https://doi.org/10.1016/j.memsci.2006.04.007.

(24) Kukizaki, M. Microbubble Formation Using Asymmetric Shirasu Porous Glass (SPG) Membranes and Porous Ceramic Membranes—A Comparative Study. *Colloids Surf. Physicochem. Eng. Asp.* **2009**, *340* (1), 20–32. https://doi.org/10.1016/j.colsurfa.2009.02.033.

(25) Ahmed, A. K. A.; Sun, C.; Hua, L.; Zhang, Z.; Zhang, Y.; Zhang, W.; Marhaba, T. Generation of Nanobubbles by Ceramic Membrane Filters: The Dependence of Bubble Size and Zeta Potential on Surface Coating, Pore Size and Injected Gas Pressure. *Chemosphere* **2018**, *203*, 327–335. https://doi.org/10.1016/j.chemosphere.2018.03.157.

(26) Oh, S. H.; Han, J. G.; Kim, J.-M. Long-Term Stability of Hydrogen Nanobubble Fuel. *Fuel* **2015**, *158*, 399–404. https://doi.org/10.1016/j.fuel.2015.05.072.

(27) Ferraro, G.; J. Jadhav, A.; Barigou, M. A Henry's Law Method for Generating Bulk Nanobubbles. *Nanoscale* **2020**, *12* (29), 15869–15879. https://doi.org/10.1039/D0NR03332D.

(28) Jadhav, A. J.; Barigou, M. Bulk Nanobubbles or Not Nanobubbles: That Is the Question. *Langmuir* **2020**, *36* (7), 1699–1708. https://doi.org/10.1021/acs.langmuir.9b03532.

(29) Jadhav, A. J.; Barigou, M. Proving and Interpreting the Spontaneous Formation of Bulk Nanobubbles in Aqueous Organic Solvent Solutions: Effects of Solvent Type and Content. *Soft Matter* **2020**, *16* (18), 4502–4511. https://doi.org/10.1039/D0SM00111B.

(30) Peyman, S. A.; McLaughlan, J. R.; Abou-Saleh, R. H.; Marston, G.; Johnson, B. R. G.; Freear, S.; Coletta, P. L.; Markham, A. F.; Evans, S. D. On-Chip Preparation of Nanoscale Contrast Agents towards High-Resolution Ultrasound Imaging. *Lab. Chip* **2016**, *16* (4), 679–687. https://doi.org/10.1039/c5lc01394a.

(31) Qin, H.; Xu, Q.; Li, W.; Dang, X.; Han, Y.; Lei, K.; Zhou, L.; Zhang, J. Effect of Stator Geometry on the Emulsification and Extraction in the Inline Single-Row Blade-Screen High Shear Mixer. *Ind. Eng. Chem. Res.* **2017**, *56* (33), 9376–9388. https://doi.org/10.1021/acs.iecr.7b01362.

(32) James, J.; Cooke, M.; Kowalski, A.; Rodgers, T. L. Scale-up of Batch Rotor-Stator Mixers. Part 2—Mixing and Emulsification. *Chem. Eng. Res. Des.* **2017**, *124*, 321–329. https://doi.org/10.1016/j.cherd.2017.06.032.

(33) Utomo, A. T.; Baker, M.; Pacek, A. W. Flow Pattern, Periodicity and Energy Dissipation in a Batch Rotor–Stator Mixer. *Chem. Eng. Res. Des.* **2008**, *86* (12), 1397–1409. https://doi.org/10.1016/j.cherd.2008.07.012.

(34) Espinoza, C. J. U.; Simmons, M. J. H.; Alberini, F.; Mihailova, O.; Rothman, D.; Kowalski, A. J. Flow Studies in an In-Line Silverson 150/250 High Shear Mixer Using PIV. *Chem. Eng. Res. Des.* **2018**, *132*, 989–1004. https://doi.org/10.1016/j.cherd.2018.01.028.

(35) Utomo, A.; Baker, M.; Pacek, A. W. The Effect of Stator Geometry on the Flow Pattern and Energy Dissipation Rate in a Rotor–Stator Mixer. *Chem. Eng. Res. Des.* **2009**, *87* (4), 533–542. https://doi.org/10.1016/j.cherd.2008.12.011.

(36) Findenegg, G. H. J. N. Israelachvili: Intermolecular and Surface Forces (With Applications to Colloidal and Biological Systems). Academic Press, London, Orlando, San Diego, New York, Toronto, Montreal, Sydney, Tokyo 1985. 296 Seiten, Preis: $ 65.00. *Berichte Bunsenges. Für Phys. Chem.* **1986**, *90* (12), 1241–1242. https://doi.org/10.1002/bbpc.19860901226.

Figure and table captions

Figure 1. Generation of BNBs in a BAS device: (a) experimental set-up; (b) different stator designs used.

Figure 2. Generation of BNBs in a SCS device: (a) experimental set-up; (b) different stator designs used.

Figure 3. Characteristics of BNB suspensions produced by BAS device with different stator designs at 10000 rpm for 30 min: (a) bubble size distribution; (b) bubble number density; (c) mean bubble diameter; (d) zeta potential.

Figure 4. Characteristics of BNB suspensions produced by SCS device with different stator designs at 10000 rpm for 30 min: (a) bubble size distribution; (b) bubble number density; (c) mean bubble diameter; (d) zeta potential.

Figure 5. Total energy dissipation as a function of operating time at 10000 rpm for each stator in (a) batch device and (b) semi-continuous device.

Figure 6. Characteristics of BNBs produced by BAS device at different rotor speeds using stator BS5 for 30 min: (a) bubble size distribution; (b) bubble number density; (c) mean bubble diameter; (d) zeta potential.

Figure 7. Characteristics of BNBs produced by SCS device at different rotor speeds using stator CS5 for 30 min: (a) bubble size distribution; (b) bubble number density; (c) mean bubble diameter; (d) zeta potential.

Figure 8. Generation of BNBs by BAS and SCS devices for different operating times using stators BS5 and CS5 at 10000 rpm: (a-b) bubble number density and (c-d) mean bubble diameter.

Figure 9. Total energy dissipation as a function of operating time and rotor speed for (a) BS5 stator in batch device and (b) CS5 stator in semi-continuous device.

Figure 10. Generation of BNBs by BAS and SCS devices at different operating temperatures and times, using stators BS5 and CS5 at 10000 rpm: (a, c) bubble number density and (b, d) mean bubble diameter.

Figure 11. Effects of additional air sparging on generation of BNBs in pure water by BAS and SCS devices using stators BS5 and CS5 at 10000 rpm for 60 min.

Figure 12. Effects of type of gas on generation of BNBs by BAS and SCS devices using stators BS5 and CS5 at 10000 rpm for 60 min: (a) bubble number density and (b) mean bubble size.

Table 1. Details of stator designs used in BAS and SCS.

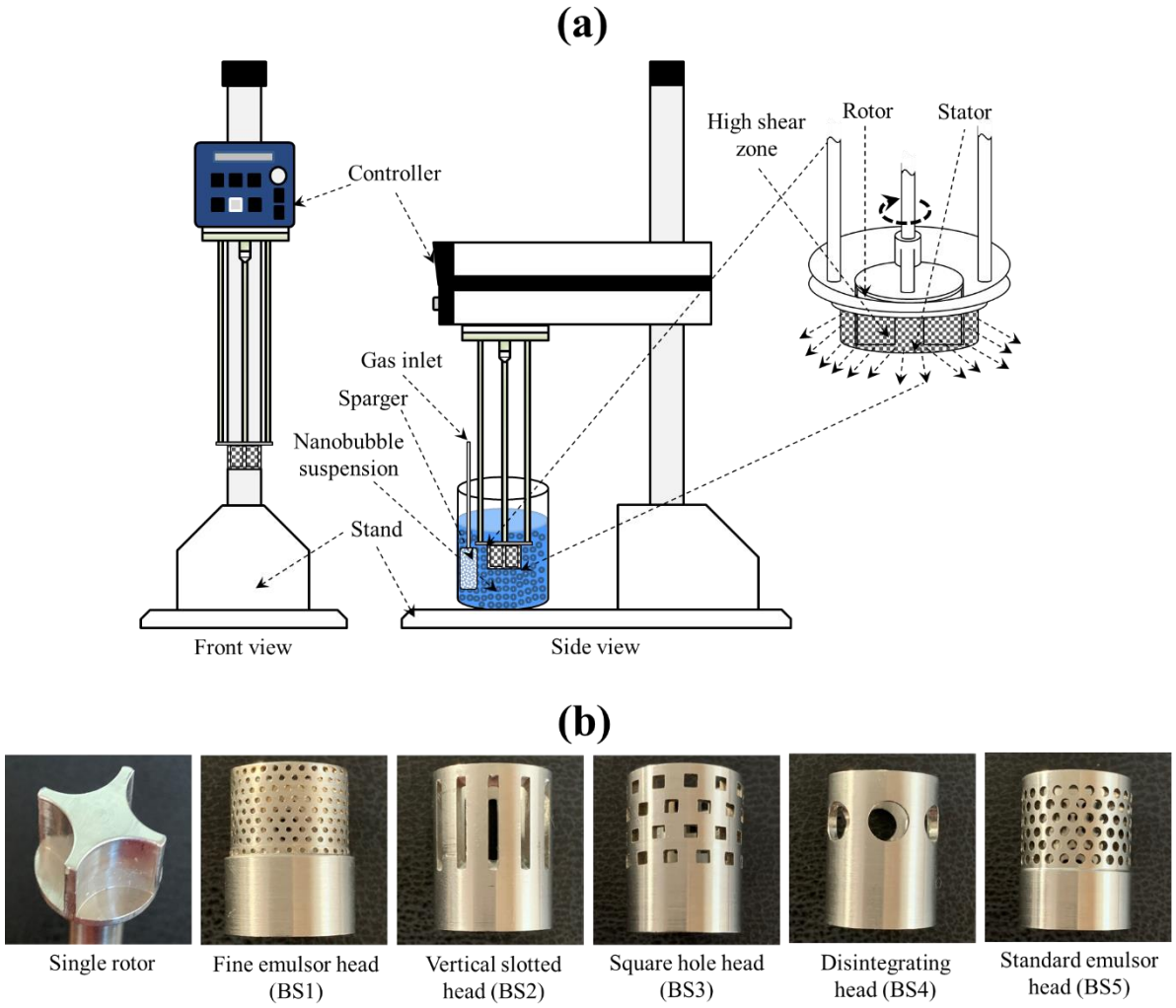

Figure 1. Generation of BNBs in a BAS device: (a) experimental set-up; (b) different stator designs used.

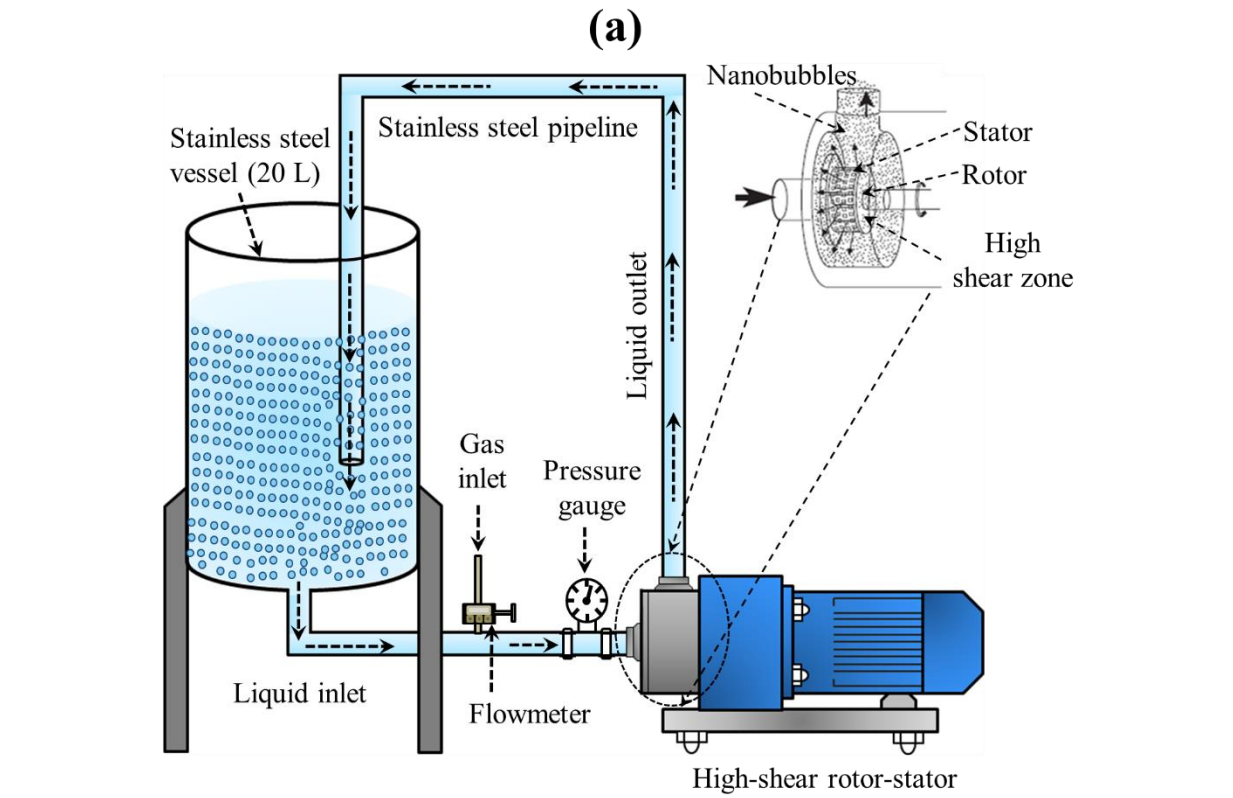

Figure 2. Generation of BNBs in a SCS device: (a) experimental set-up; (b) different stator designs used.

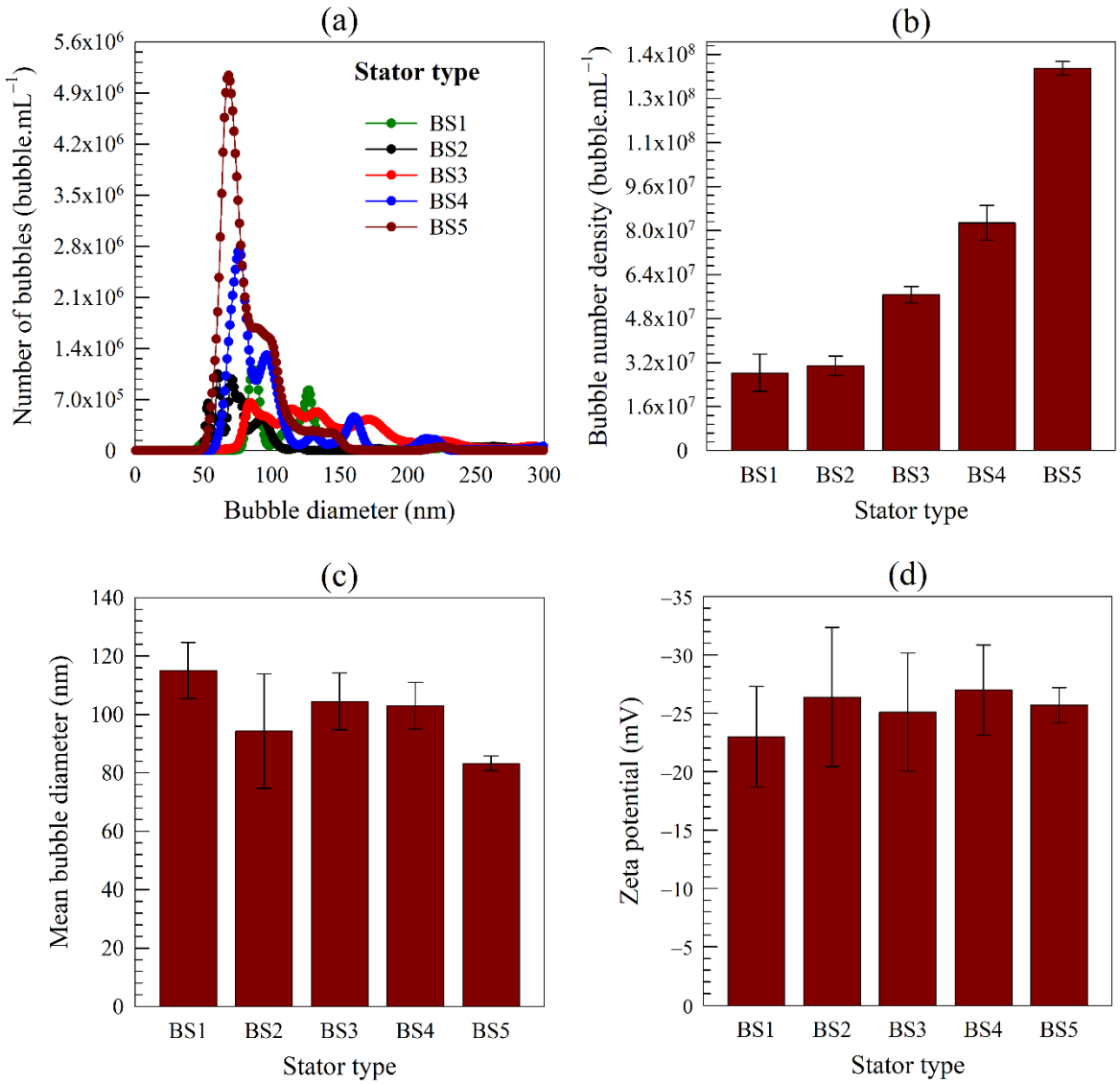

Figure 3. Characteristics of BNB suspensions produced by BAS device with different stator designs at 10000 rpm for 30 min: (a) bubble size distribution; (b) bubble number density; (c) mean bubble diameter; (d) zeta potential.

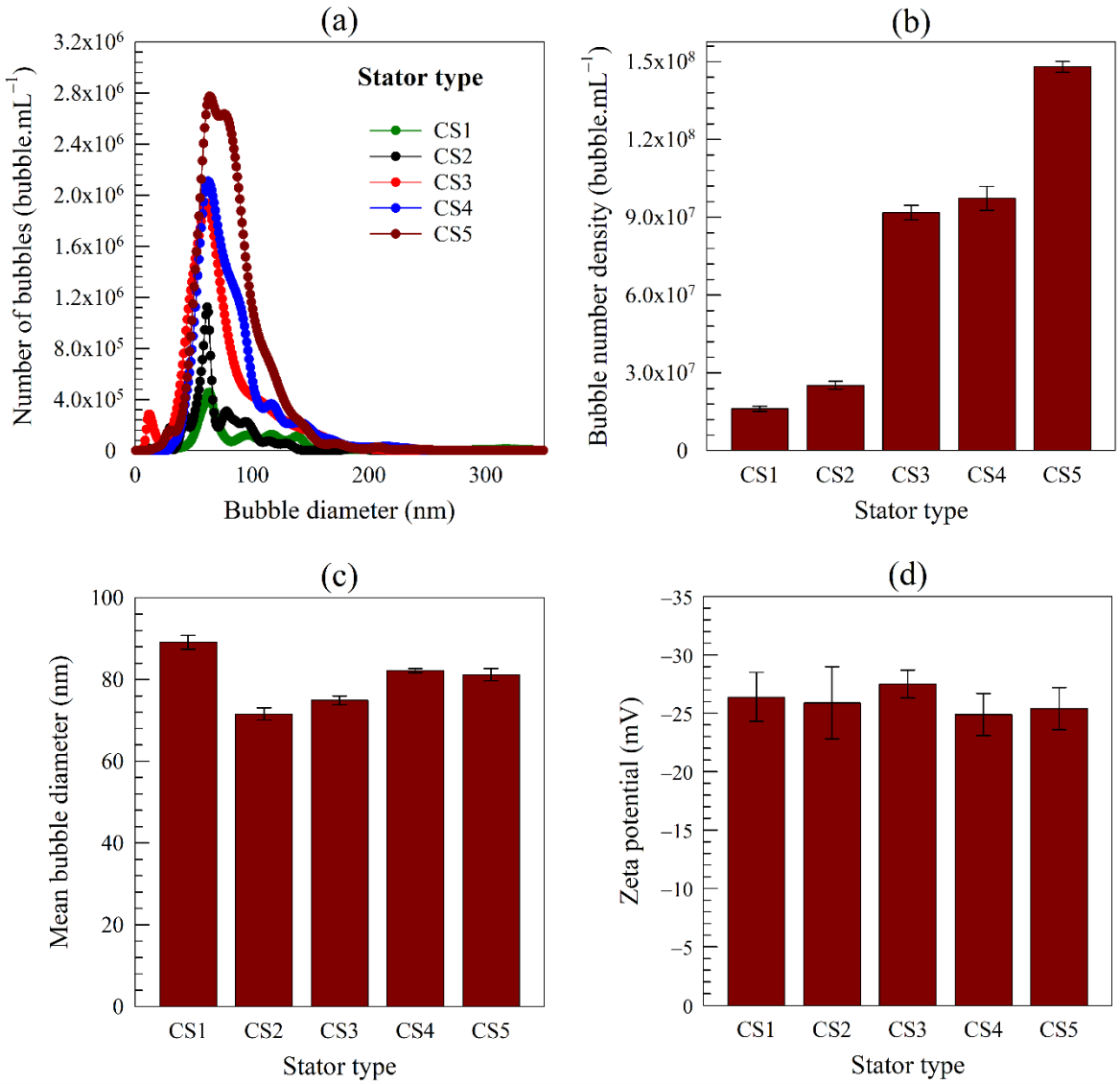

Figure 4. Characteristics of BNB suspensions produced by SCS device with different stator designs at 10000 rpm for 30 min: (a) bubble size distribution; (b) bubble number density; (c) mean bubble diameter; (d) zeta potential.

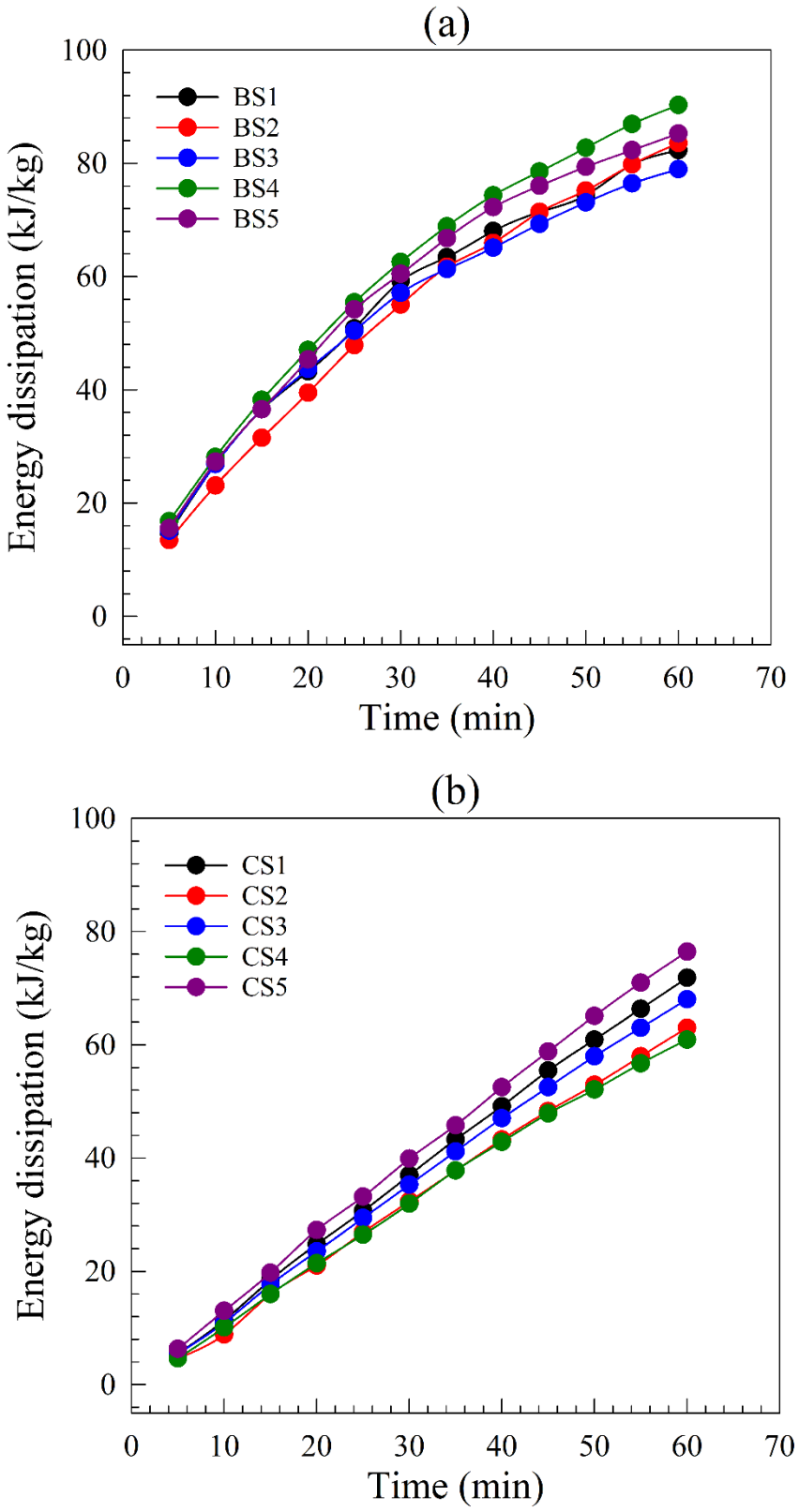

Figure 5. Total energy dissipation as a function of operating time at 10000 rpm for each stator in (a) batch device and (b) semi-continuous device.

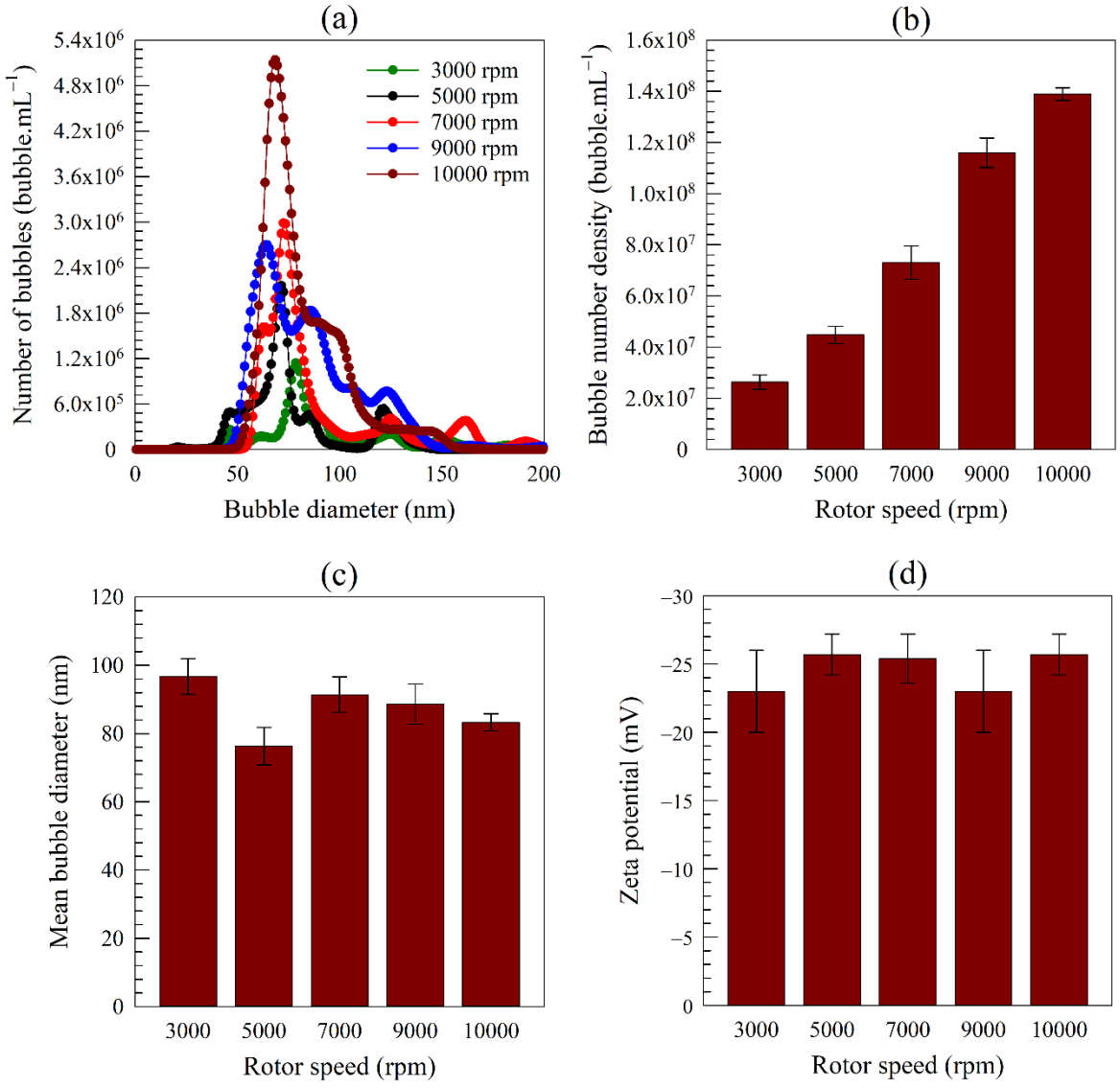

Figure 6. Characteristics of BNBs produced by BAS device at different rotor speeds using stator BS5 for 30 min: (a) bubble size distribution; (b) bubble number density; (c) mean bubble diameter; (d) zeta potential.

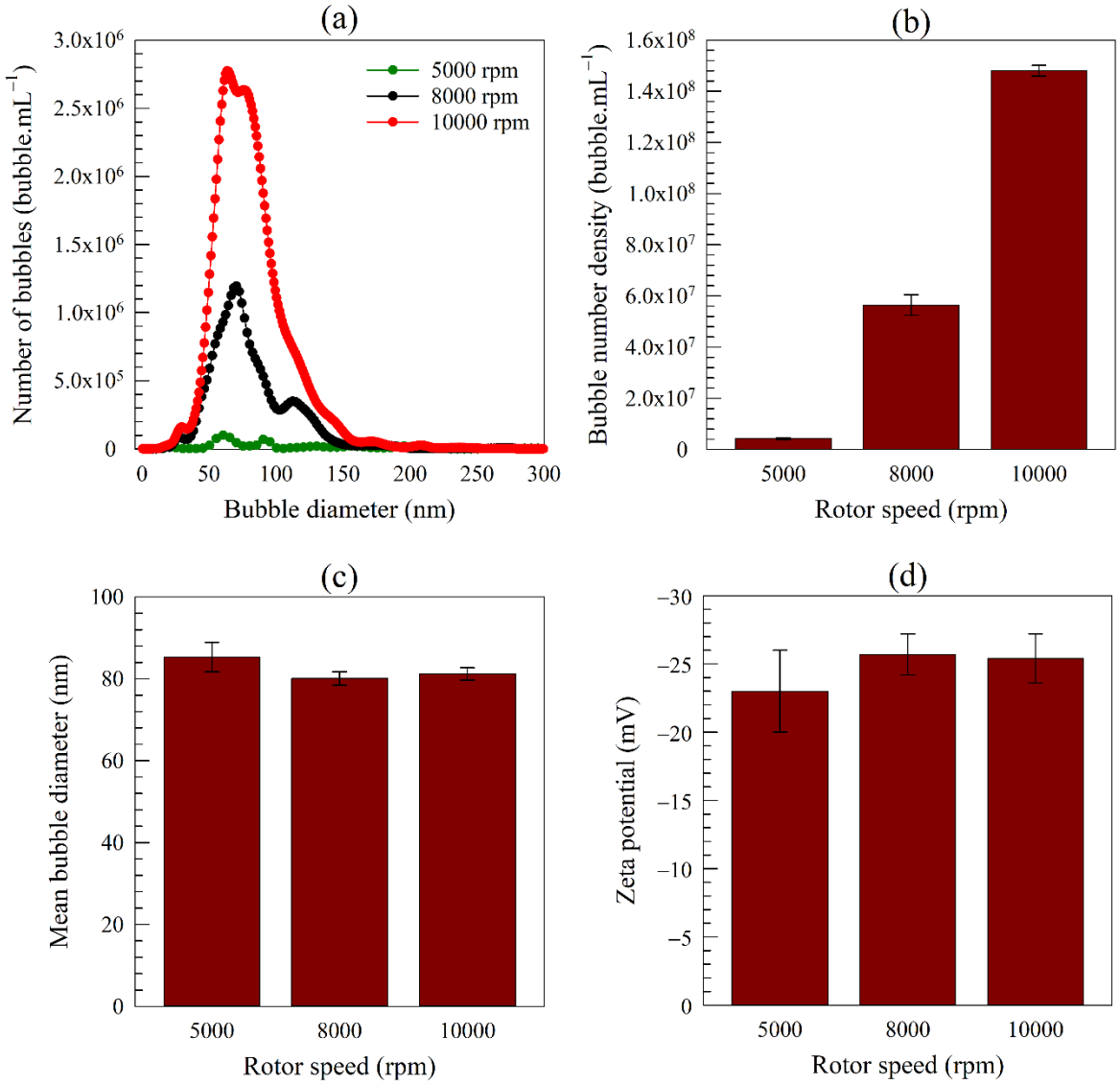

Figure 7. Characteristics of BNBs produced by SCS device at different rotor speeds using stator CS5 for 30 min: (a) bubble size distribution; (b) bubble number density; (c) mean bubble diameter; (d) zeta potential.

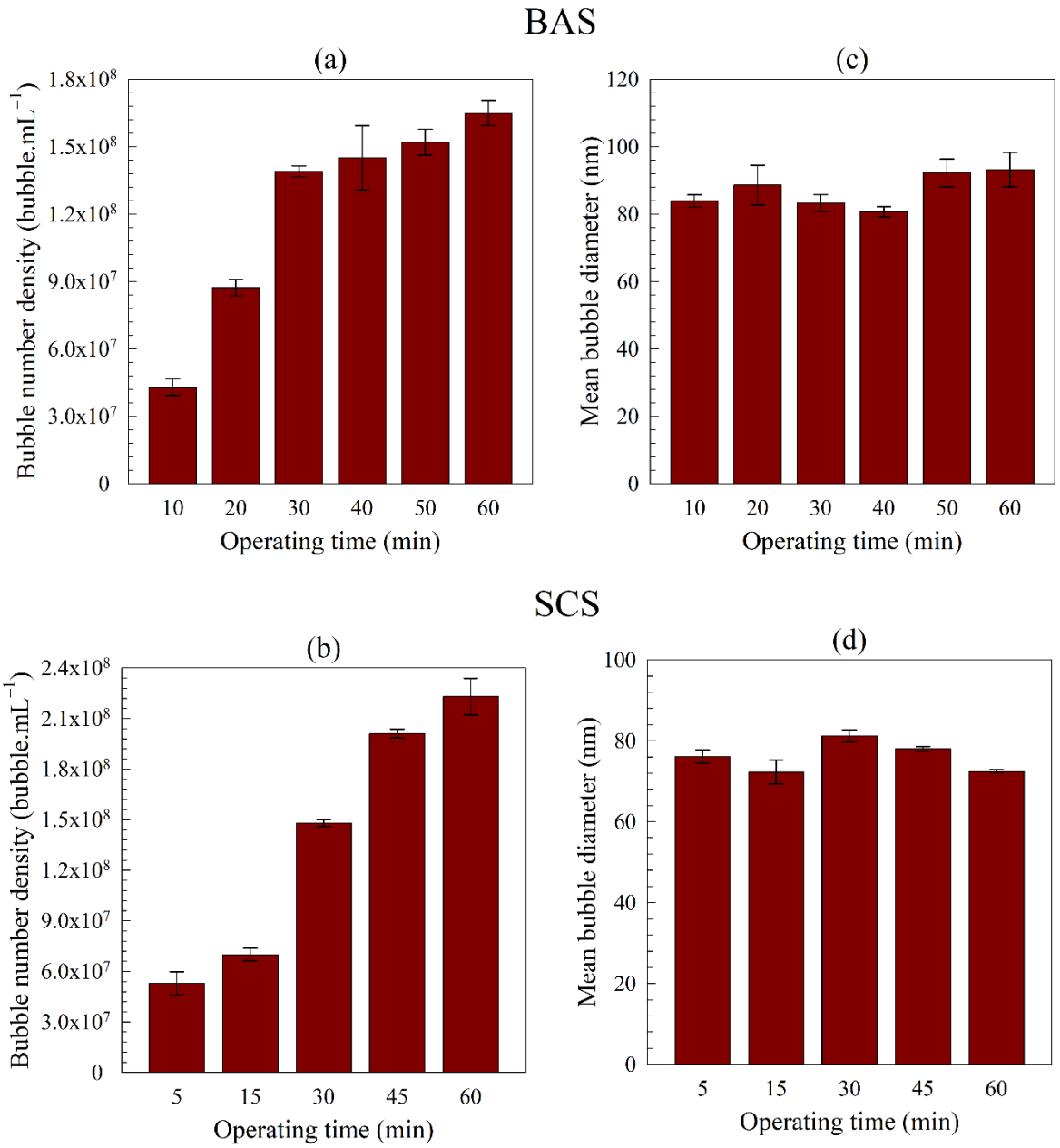

Figure 8. Generation of BNBs by BAS and SCS devices for different operating times using stators BS5 and CS5 at 10000 rpm: (a-b) bubble number density and (c-d) mean bubble diameter.

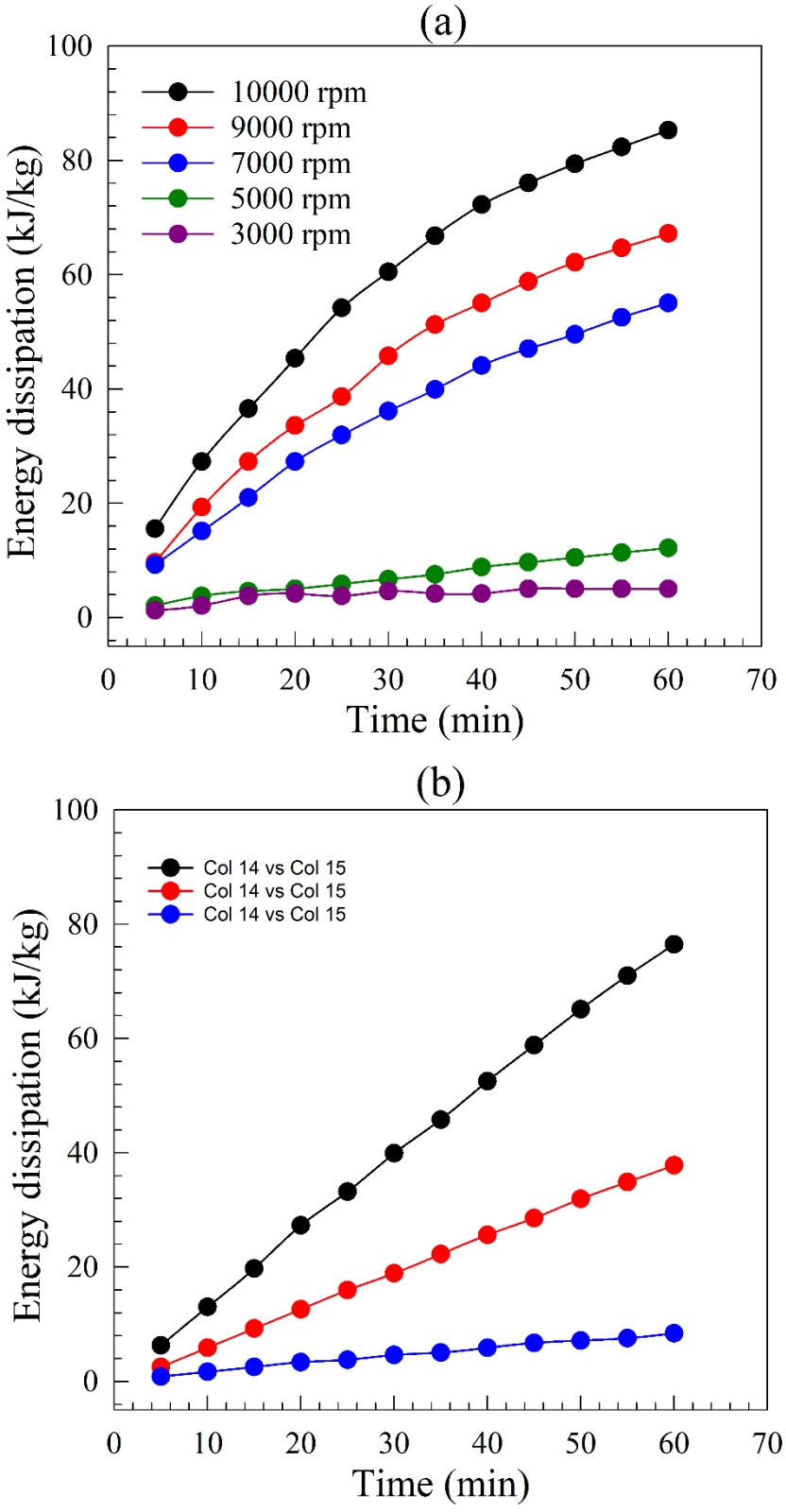

Figure 9. Total energy dissipation as a function of operating time and rotor speed for (a) BS5 stator in batch device and (b) CS5 stator in semi-continuous device.

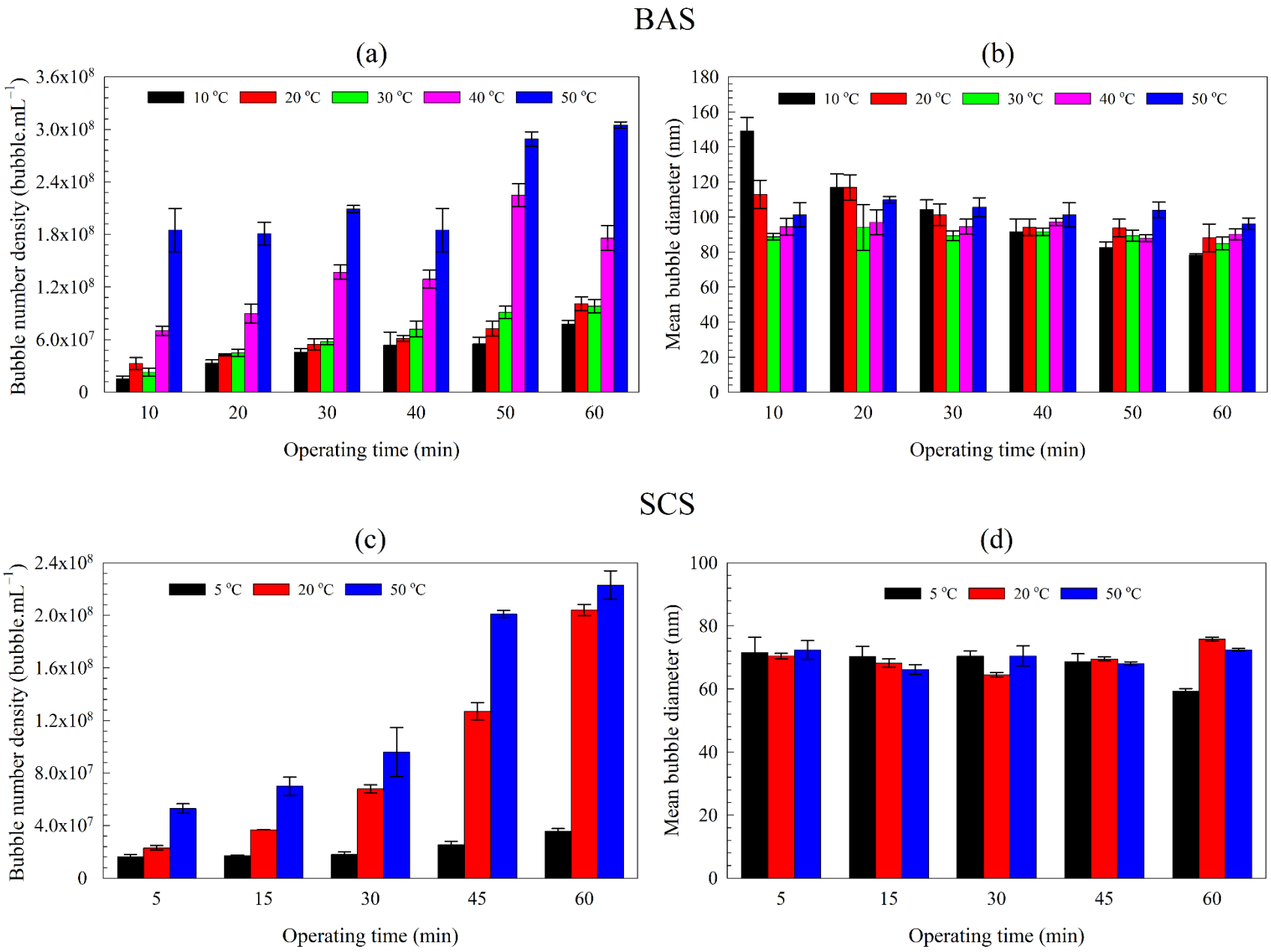

Figure 10. Generation of BNBs by BAS and SCS devices at different operating temperatures and times, using stators BS5 and CS5 at 10000 rpm: (a, c) bubble number density and (b, d) mean bubble diameter.

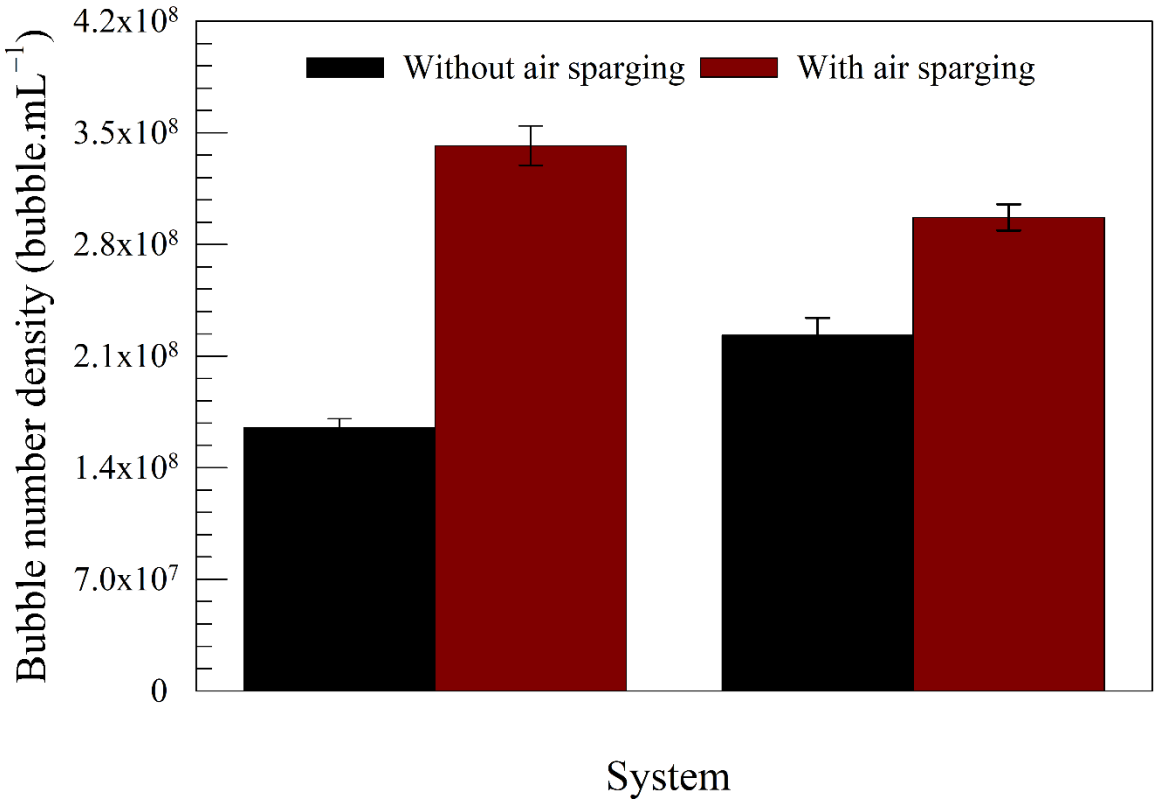

Figure 11. Effects of additional air sparging on generation of BNBs in pure water by BAS and SCS devices using stators BS5 and CS5 at 10000 rpm for 60 min.

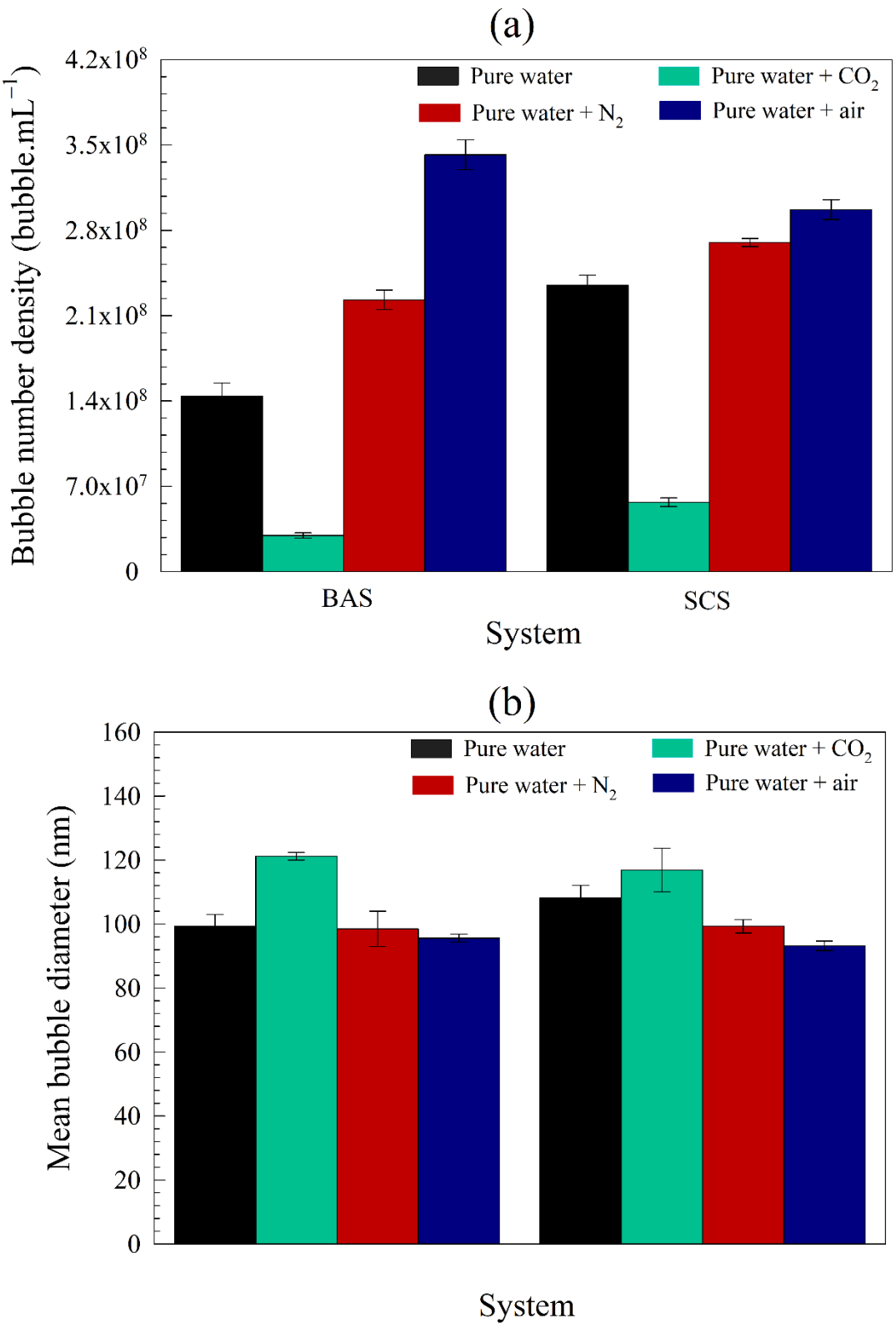

Figure 12. Effects of type of gas on generation of BNBs by BAS and SCS devices using stators BS5 and CS5 at 10000 rpm for 60 min: (a) bubble number density and (b) mean bubble size.

Table 1. Details of stator designs used in BAS and SCS.

Type	Number of openings	Length of opening (mm)	Area of opening (mm^2)	Total Area of opening (mm^2)
Batch high shear rotor-stator device system (BAS)				
Fine emulsor head (BS1)	270	0.94	0.7	187.37
Vertical slotted head (BS2)	12	1.7 × 11.92	20.26	243.16
Square hole head (BS3)	48	2.4 × 2.4	5.76	276.48
Disintegrating head (BS4)	6	8.0	50.27	301.62
Standard emulsor head (BS5)	138	1.7	2.27	313.23
Semi-continuous high shear rotor-stator device system (SCS)				
Square hole head (CS1)	96	2.0 × 2.0	4.0	384
Slotted disintegrating head (CS2)	20	3.20 × 10.25	32.8	656
Slotted disintegrating high shear screen head (CS3)	60	0.5 × 10.25	5.13	307.5
Emulsor screens head (CS4)	576	0.5	0.2	115.2
General purpose disintegrating (CS5)	8	10.25	82.52	660.1

For Table of Contents Only